Formation of clay minerals on Mars: insights from long-term experimental weathering of olivine

A. Gaudin, E. Dehouck, O. Grauby, N. Mangold

Formation of clay minerals on Mars: insights from long-term experimental weathering of olivine

A. Gaudin[a], E. Dehouck[b,c], O. Grauby[d], N. Mangold[a]

[a] *Laboratoire de Planétologie et Géodynamique de Nantes (LPGN), CNRS/Université de Nantes, 44322 Nantes, France*

[b] *IRAP, Université de Toulouse, CNRS, UPS, CNES, Toulouse, France*

[c] *Present adress : Laboratoire de Géologie de Lyon : Terre, Planètes, Environnement, UMR 5276, CNRS, Université Lyon 1, ENS Lyon, Villeurbanne, France*

[d] *Centre Interdisciplinaire de Nanoscience de Marseille (CINaM), CNRS/Aix-Marseille Université, Campus de Luminy, 13288 Marseille, France*

keywords:

Mars, surface

Mars, atmosphere

Mineralogy

Abstract

Laboratory experiments are useful to constrain the environmental parameters that have allowed the formation of the ancient hydrous mineralogical assemblages observed at the surface of Mars, which are dominated by ferric smectites. Weathering under a dense CO_2 atmosphere on early Mars is a process frequently invoked to explain their formation but has proven difficult to test in the laboratory due to low reaction rates. Here, we present a long-term weathering experiment (470 days, 45°C) of forsteritic olivine specially designed to increase as much as possible the amount of reaction products and thus allow their detailed SEM/TEM petrological and chemical characterization. Our results show the formation of crystalline smectites both under 1 bar of CO_2 and under ambient air. However, important

differences are observed between the two types of conditions. The smectite formed under CO_2 has an average chemical formula per half unit-cell of $Si_{3.92}Al_{0.16}Fe^{3+}_{0.78}Mg_{1.66}Cr_{0.01}Ni_{0.06}K_{0.04}Ca_{0.04}.O_{10}(OH)_2$. It is thus intermediate between a trioctahedral Mg-rich saponite and a dioctahedral ferric smectite. It is also clearly enriched in Fe compared its counterpart formed under ambient air ($Si_{3.68}Al_{0.12}\mathbf{Fe^{3+}_{0.37}}Mg_{2.61}Cr_{0.01}Ni_{0.02}K_{0.04}Ca_{0.25}.O_{10}(OH)_2$). This result demonstrates that the enrichment in Fe observed for Martian smectites is to be expected if they were formed by low-temperature weathering under a dense CO_2 atmosphere. Another difference is the nature of the accompanying phases, which includes amorphous silica (in the form of opal spheres 10 to 100 nm in diameter) and Mg-carbonates under CO_2, but are limited to rare kaolinite under ambient air. The observation of kaolinite particles and the significant amount of Al measured in smectites despite the Al-poor nature of the initial material shows that this element is easily concentrated by low-temperature processes. The concentration of this element by weathering could lead to the formation of Al-rich upper horizons, as frequently observed on Mars.

1. Introduction

Several lines of evidence point toward the presence of an active hydrosphere on early Mars. These lines of evidence include the extensive networks of fluvial valleys (e.g., Craddock and Howard, 2002; Hynek et al., 2010), the highly degraded impact craters (e.g., Craddock et al., 1997; Mangold et al., 2012) and the widespread secondary minerals, dominated by Fe/Mg-smectites (e.g., Poulet et al., 2005; Carter et al., 2013). However, the implications of all these observations for the nature of the early Martian climate have been – and continue to be – the subject of intense debate. For example, it has been proposed that a large fraction of the Martian clay minerals were formed in the subsurface by hydrothermal

groundwater circulation and thus that the conditions at the surface were not necessarily very different from today (e.g., Ehlmann et al., 2011). In turn, numerous vertical sections of Al-rich clays overlying Fe/Mg-smectites, a setting typical of terrestrial weathering profiles (e.g., Gaudin et al., 2011), have been observed in various regions of the planet and interpreted as a strong evidence for low-temperature, near-surface aqueous alteration of the crust, and thus for a warmer and wetter climate (e.g., Carter et al., 2015).

More recently, the detailed monitoring of the Martian upper atmosphere by the MAVEN (Mars Atmosphere and Volatile EvolutioN) mission has provided the first reliable estimates of cumulative atmospheric escape over the history of the planet (Jakosky et al., 2017). These results indicate that Mars has lost several tenths of bars to a few bars of CO_2 over the last 4 billion years, as well as several meters to several tens of meters GEL (global equivalent layer) of H_2O (Jakosky et al., 2017). Therefore, independently from the difficulties to generate a warm and wet climate using GCMs (global circulation models; e.g., Forget et al., 2013), the observational evidence – from both the surface and now the upper atmosphere – point toward extensive interactions between the early Martian crust, an active hydrosphere and a relatively thick CO_2 atmosphere. Nevertheless, many long-standing questions related to the duration, amplitude and exact geochemical conditions (e.g., pH, redox) of early Mars surface alteration remain largely unresolved. Yet, low-temperature weathering is not a process that has been thoroughly explored by laboratory experiments using relevant conditions (i.e., CO_2 atmosphere) and starting materials (i.e., basaltic silicates). Here, we present new experimental results obtained under such conditions in order to better understand the weathering processes that occurred at the surface of Mars.

2. Background: experimental alteration under Mars conditions

Laboratory experiments are useful to constrain the environmental parameters that would (or would not) have allowed the formation of the ancient mineralogical assemblages observed at the Martian surface by orbital and in situ missions. However, most experimental studies aiming at recreating Mars' secondary mineralogy have focused so far on conditions producing fast reaction rates, such as low pH (e.g., Chevrier et al, 2004; Tosca et al., 2004; Dehouck et al., 2012; Marcucci and Hynek, 2014) and/or high temperature (>100 °C ; e.g. Schröder et al., 2004; Peretyazhko et al. 2016). These studies thus provide information about acid-sulfate and/or hydrothermal processes, but not about aqueous alteration in milder conditions, referred here as weathering. Similarly, in the context of Earth's climate change mitigation, there are numerous experimental studies of the "carbonation" of primary silicates such as olivine (e.g., Giammar et al., 2005; Bearat et al., 2006; Gerdemann et al., 2007; Daval et al., 2011), but again these studies are generally carried out in conditions favoring fast reaction rates (T >100 °C and/or pCO_2 >100 bars) and are thus not applicable to planetary surficial processes. Overall, the search for fast reaction rates has biased the experimental literature toward short-term alteration processes, even though long-term processes such as weathering have been equally (if not more) important in creating secondary mineralogical assemblages typically observed on Mars, in particular those involving several varieties of clay minerals.

In the past years, our group has developed a series of laboratory experiments to fill this gap in the experimental knowledge of alteration (Table 1). Low-temperature weathering experiments using olivine and pyroxenes as starting materials were described by Dehouck et al. (2012, 2014a, 2016) and showed that a reaction predicted by geochemical modeling to produce predominantly carbonates could instead produce smectite clays and amorphous silica.

The first series of experiments were carried out over 4 years at room temperature in rock-dominated conditions (i.e., at low liquid/rock ratio) and showed interesting differences in

chemical pathways (Dehouck et al., 2016). In particular, it was observed that the addition of an oxidizing compound (H_2O_2) under CO_2 could inhibit the formation of smectites and favor the formation of carbonates – and conversely when the environment is anoxic. These results thus strongly suggest that anoxic conditions were required to form the widespread Fe/Mg-smectites through weathering of the Martian basaltic crust under a CO_2 atmosphere (Dehouck et al., 2016). Moreover, Dehouck et al. (2014a) studied the alteration of forsteritic olivine under CO_2 in water-dominated conditions (i.e., at a liquid/rock ratio of 10). After three months of reaction, the samples exposed to anoxic conditions showed the development of significant amounts of a silica-rich phase as well as Mg-rich smectites on the olivine grains, and only traces of carbonates, whereas the samples exposed to CO_2 and H_2O_2 produced only the silica-rich phase.

Unfortunately, in the two studies described above, the low abundance of the secondary products (especially smectites) hindered their detailed chemical and SEM/TEM petrographic characterization. This may have been due, in part, to the absence of continuous stirring (the reactors were only stirred manually a few times per week in the work of Dehouck et al., 2014a). Therefore, building from our experience, we conducted a new experiment similar in principle to the one presented by Dehouck et al. (2014a), but specially designed to increase as much as possible the amount of reaction products, with the hope of being able to investigate in more details their nature and properties. Specifically, our new experimental setup allowed us to weather forsteritic olivine in a CO_2 glove box (1) with continuous stirring of the reactors and (2) during 470 days, which is more than five times longer than the study of Dehouck et al. (2014a). The chemistry, mineralogy and petrography of the altered samples were characterized by means of near-infrared spectroscopy (IR), X-Ray diffraction (XRD), thermogravimetric analyses (TGA) and scanning and transmission electron microscopy (SEM and TEM), as detailed in Appendix 1.

3. Starting material and experimental setup

As a starting material, we selected a natural sample of forsteritic (Fo_{90}) olivine. Olivine is a common component of ultramafic and mafic rocks, from which the martian crust is mainly made. It has been unambiguously detected in various regions of Mars based on orbital data (Hoefen et al., 2003; Mustard et al., 2005; Poulet et al., 2007; Ody et al., 2013). Moreover, among the secondary minerals discovered so far in olivine-rich regions of Mars (Mangold et al., 2007; Ehlmann et al., 2009; Gaudin et al., 2011; Bishop et al., 2013), several species of phyllosilicates (smectites, serpentines) and carbonates (magnesite, hydromagnesite) are known to derive from olivine or olivine-bearing rocks in terrestrial environments (e.g., Delvigne et al., 1979; Velbel et al., 1991; Wilson, 2004). Finally, forsteritic olivine is weakly resistant to weathering, but it is also sufficiently common on the surface of the Earth – as opposed to fayalitic olivine, in particular – to be found in "fresh" state and in sufficient amount to meet the requirements of this study.

The forsteritic olivine used in this study originated from San Carlos, Arizona (USA) and consisted of olive-green, centimeter-sized monocrystals (De Hoog et al., 2010). The cleanest grains were selected from the original lot and minor bright impurities macroscopically visible on the surface of some grains were removed using a diamond-covered abrasion tool. The grains were then cleaned using an ultrasonic bath in ethyl alcohol and finely crushed using an automatic crusher with agate balls. The resulting, white-colored powder was homogenized and sieved to obtain a <65 µm fraction. To monitor the purity of the olivine powder before the experiment, we performed a precise mineralogical and chemical characterization using powder X-ray diffraction, near-infrared spectroscopy, inductively-coupled plasma optical emission spectroscopy (ICP-OES) and TEM-EDX (energy-dispersive X-ray) analyses. The XRD pattern showed no crystalline phase other than olivine. The near-infrared spectrum shows minute absorption bands at 1.9 and 2.31 µm attributed to a Mg-rich smectite, which indicates that this olivine was slightly altered in the field before collection

(Fig. 2). Chemical analyses of the bulk powder by ICP-OES and of individual particles by TEM-EDX both indicate a Fo90 composition. Trace elements were also measured by ICP-OES using standard addition method and indicate contents in Mn, Ca, Al, Cr, Co and Na close to those reported by De Hoog et al. (2010) for the San Carlos olivine (Table 2).

Two alteration experiments were carried out from the olivine. The first one was conducted under a pure CO_2 atmosphere (1 bar) in a glove box (Mbraun-LABstar) and the second one was conducted outside the glove box, under ambient air. The glove box is equipped with an electrochemical oxygen analyzer (MB-OX-EC-PLC, 1-1000 ppm O_2) and a single-column, fully automatic and regenerable CO_2 purification system that maintains atmosphere levels of oxygen and moisture below 1 ppm. The reactors used were 60-mL glass bottles, in which 20 mL of ultrapure water were added to 2 g of powdered forsteritic olivine, giving a liquid-to-rock (L/R) ratio of 10. Basing on our previous experiments presented in Dehouck et al. (2014) where a blank experiment with only ultrapure water in a glass bottle was performed, we assume here a negligible effect of the dissolution of the glass bottle on the chemistry of the solutions, and therefore on the alteration of the olivine. Before the start of the experiment, the ultrapure water was placed in the glove box for 2 hours and continuously stirred in order to remove dissolved oxygen. The reactors were heated – so as to obtain a solution temperature of 45 °C – and stirred during the full 470 days of the experiment using a hotplate placed on top of an orbital agitator (IKA KS260 basic) (Fig. 1). At the end of the experiment, pH and Eh values of each solution were measured; then, the CO_2 sample was dried in the glove box at ambient temperature, whereas the air sample was dried in an oven at 29 °C. Note that the experimental setup used by Dehouck et al. (2014a) did not allow to dry the samples under CO_2 and that vacuum-drying was used instead.

Our experiments, closed environments with a low L/R ratio, were designed to reproduce the first stage of weathering at the alteration front of the profile, where drainage and leaching conditions are low and where Fe/Mg smectite is formed. Concerning the relatively “high” temperature used in these experiments to simulate weathering, we assume that a temperature increase from a room temperature to 45°C has an effect on the kinetics but not on the reaction pathways. The duration of our experiment is very short compared to a natural geological context of weathering. Therefore, we consider here the temperature, in the 15-50°C range, as a proxy of time. Thereby, the value of 45°C was chosen as a compromise between two opposite requirements: (1) increasing reaction rates to maintain the experiment in a reasonable timeframe and (2) keeping realistic conditions for surface aqueous processes.

5. Results

5.1. Bulk analyses

pH and Eh of the solutions. Measurements of pH and Eh values were performed at the end of the experiment after 470 days of reaction. Results indicate, as expected, a more acidic solution for the CO_2 reactor with a pH value of 6.76 against a pH of 8.6 for the air one. Concerning Eh, a value of -46 mv is measured for the CO_2 reactor, indicating a reducing environment, and a value of 220 mv is measured for the air one, indicating an oxidizing environment.

Near-infrared spectroscopy. The near-infrared spectra obtained from the weathered samples compared to the initial one indicate only slight spectral modifications with an overall shape still typical of olivine, in particular with an intense and broad Fe^{2+}-related composite band at 1.04 µm (Fig. 2a).

In the 1.7-2.6 µm region (Figs 2b, c), the modifications observed for the CO_2 sample consist of a significant increase of the 1.9-µm band, classically attributed to bound or interlayer water. This suggests the formation of hydrated phases during the experiment. Moreover, we observe the appearance of a broad and asymmetrical band between 2.20 and 2.26 µm, attributed to a Si-OH vibration in silica (e.g. McKeown et al., 2011). An asymmetrical band at 2.31 µm with a slight shoulder near 2.29 µm are also observed and are assigned to trioctahedral Mg_3-OH in a Mg -rich smectite (Cuadros et al., 2016). The shallow band at 2.39 µm is also consistent with a Mg -bearing smectite (Fig. 2b-c). Finally, the 3.5-4.2 µm region (Figs. 2d, e) displays the appearance of a broad and deep band at 3.96 µm with a shoulder at 3.82 µm, which is attributed to Mg-carbonates, most likely to hydromagnesite ($Mg_5(CO_3)_4(OH)_2{\cdot}4H_2O$). It is possible that the shallow absorption band at 2.5 µm is also related to this carbonate.

Concerning the air sample, the absorption bands at 1.9, 2.29, 2.31 and 2.39 µm appear much more intense and better resolved than those described for the CO_2 sample, indicating a larger amount of Mg-rich smectite formed in this experiment. Note that sharp bands at 2.69 µm and 2.72 µm are also identified and attributed to Mg-OH stretching vibrations in smectites (Pelletier et al., 1999). Moreover, the band at ~2.2 µm has a different shape and is shifted toward shorter wavelengths compared to that of the CO_2 sample. Therefore, here we interpret this band as due to Al_2-OH environment in smectite (e.g. Bishop et al., 2011) rather than silica (Fig. 2b, c). However, as some particles of kaolinite were detected by TEM (see below), a minor contribution of Al-OH related to this mineral cannot be ruled out but remains indistinguishable (absence of the characteristic doublet near 2.2µm). Lastly, no spectral feature of carbonate is detected in the 3.5-4.2 µm region (Figs. 2d, e).

Thermogravimetric and differential thermal analysis (DTA). TGA and DTA curves of the initial olivine and of the CO_2 and air samples are presented in figure 3. A different thermal

behavior between the three samples is observed. No significant loss mass is detected for the unaltered olivine. For the air sample, a total mass loss of about 0.7 % is measured from 17 to 800 °C, with a first rapid mass loss near 70 °C, followed by a slower gradual mass loss between 100 and 800 °C. In agreement with the smectite previously detected by IR in this sample, and as reported by Kooli and Jones (1997) for saponites, the first mass loss (-0.4 wt %) is interpreted as due to the loss of phisisorbed and interlayer water and the slower mass loss between 100 and 800 °C as due to gradual dehydroxylation of the smectites No rapid mass losses due to dehydroxylation of clay minerals are here measured. Thereby, dehydroxylation is expected to occur near 800-850°C for a saponite, 300-500°C for a nontronite, 700°C for a montmorillonite and 530-500°C for a kaolinite (e.g. Cuadros et al., 2013, Földvári 2011). Notice that the range of temperature (0-800°C) used for our analyses does not allow to detect the dehydroxylation of a saponite. TheCO_2 sample curve shows a total mass loss of 2.1 %, with three regions of rapid mass loss. The first one (-0.8 wt %), between 20 and 250 °C, is accompanied by a H_2O release and is likely due to the combined dehydration of smectite, silica and carbonate previously detected by IR. As for the air sample, it is probable that a gradual dehydroxylation of the smectite also occurs between 100 and 800 °C. The two other rapid mass losses (-1.3 wt %) near 425 and 515 °C are accompanied by a CO_2 release and appear consistent with the occurrence of hydromagnesite previously detected by IR and with thermal data reported in Montoya et al. (2003) for this mineral. Since a pure hydromagnesite contains 37.65 wt % of CO_2 and that the delta mass due to the CO_2 release measured in this sample is of 1.3 wt %, the abundance of hydromagnesite is here estimated at 3.45 wt %.

XRD mineralogy. No significant mineralogical change before and after the experiment is detected by XRD, both in the CO_2 sample and the air one (Fig. 4). The amount of alteration products is too low to allow their detection by this method.

5.2. Microscopic observations and analyses

Petrological observations of altered olivine grains by SEM and TEM show significant modifications of their surfaces, both for the CO_2 sample and the air sample. However, the nature of these modifications differ between the two samples.

CO_2 sample. The surfaces of olivine grains altered under CO_2 display the development of numerous silica spheres with a diameter comprised in most cases between 10 and 100 nm (Figs. 5c, d, e, 6) (e. g., "An 1" TEM-EDX data located in Fig 6 and reported in a Si-Fe-Mg diagram (Fig. 8)). These particles are similar to those described in natural opals both in terms of morphology and size (e.g. Fritsch et al., 2006; Rondeau et al., 2004). Their presence is also consistent with the Si-OH infrared band previously reported for this sample. The spheres appear either isolated and randomly dispersed (Fig. 5d), or juxtaposed and coalescing to form larger layers (Fig. 5c). Some partially organized stacking of the silica spheres are sometimes observed, especially along the break planes of olivine grains, and occurrences of bridges linking neighboring spheres are also noted (Fig. 5d). Detailed high-resolution TEM (HRTEM) observations coupled with acquisition of micro-diffraction patterns of these spheres show no fringe lattice and no diffraction spots or rings, indicating the amorphous character of this material (Figs. 6a, b).

Moreover, the surface of olivine grains show more locally the development of thin flaky particles, which are interpreted as Mg/Fe-rich smectite particles based on their typical morphology and in agreement with IR and TEM-EDX data. Their detailed chemical compositions are displayed in table 3 and reported in the Fig. 8 (e.g., "An 6" TEM-EDX data located in Fig 6 and reported in Fig. 8, Table 3) . These clay minerals are developed either directly on the olivine surfaces (Fig. 5b, 6c), or as coatings around the silica spheres described above (Figs. 5e, 6a). The HRTEM study of the smectite flakes reveals very diffuse boundaries

and blurred 001 fringes with numerous discontinuities. Most of the crystallites oriented perpendicularly to c* display fewer than 5 stacked layers. The measured (001) d spacing values vary between 12 and 13 Å (Fig. 6c) and are thus typical of smectite structure (e. g. Brindley and Brown, 1980). These observations demonstrate that despite their low crystallinity, the flakes are true smectites and not amorphous precursors. Finally, we observed the occurrence of Mg-rich carbonate particles with minor iron, which is consistent with the hydromagnesite detected by infrared spectroscopy in this sample (Fig. 5f).

Air sample. The olivine grains altered under ambient air appear almost entirely coated by flakes of Mg/Fe smectites (Fig. 7a-e, Fig. 8, Table 3) (e. g., "An 8" TEM-EDX data located in Fig. 7 and reported in Fig. 8, Table 3) . These are clearly more extensively developed than previously described for the CO_2 sample. At higher magnification by SEM, it can be seen that smectites display a typical honeycomb structure (Fig. 7 a, b). The HRTEM study of the flakes again reveals very diffuse boundaries and blurred 001 fringes with numerous discontinuities and d spacing values varying between 12 and 13 Å (Fig. 7d). We also observed some very small isolated pseudo-hexagonal particles, which could be interpreted as kaolinite ("An 25, 33" in table 3 and reported in Fig. 8) (Fig. 7f). Finally, no carbonate or silica particles were detected in this sample.

Chemistry of the secondary products. TEM-EDX analyses of clay particles and silica-rich spheres formed in the altered samples are reported in Si-Fe-Mg and Si-(Fe+Mg)-Al diagrams (Fig. 8). Since these phases have small sizes (<100 nm) and are developed as thin coatings around olivine grains, numerous compositions actually correspond to mineralogical mixtures and only a few particles were interpreted as "pure" (Fig. 8). For the CO_2 sample, both Si-rich spherical particles and flaky Mg/Fe-rich smectite particles are detected, whereas

in the air sample, abundant flaky Mg/Fe-smectites are again detected but some rare Al-rich particles interpreted as kaolinite are also observed (Figs. 8b, c).

The flaky smectites show intermediate compositions between a Mg-rich saponite and a ferric smectite end-member (Figs. 8a, b). This is coherent with the characteristic doublet at 2.29-2.31 µm of a saponite observed in the IR spectra, and where the $(Fe^{3+})_2$□-OH contribution near 2.29 µm would be masked by the Mg_3-OH vibrations (see nontronite and saponite spectra form USGS reported in Fig. 2). Moreover, as already reported in Dehouck et al. (2014a), a clear enrichment in iron is noted for the smectites formed under CO_2 compared to those formed under ambient air (Fig. 8b). We did not observe isolated Fe-smectite or Mg-smectite endmembers, which suggests that the intermediate compositions measured are due to substitutions of $Fe^{3+}Fe^{3+}$□ (□: vacant site) for $Mg^{2+}Mg^{2+}Mg^{2+}$ clusters within the smectite layers rather than a mechanical mixing of dioctahedral and trioctahedral smectite particles or layers.

Individual and average chemical formulae of smectite particles are presented in Table 3. They are calculated for $O_{10}(OH)_2$, assuming that Fe is in the ferric state (as expected from figure 8 and IR data). The formulae show that Mg^{2+} is the dominant octahedral cation: it varies from 1.61 to 1.76 per half unit-cell for the CO_2 smectites and from 2.37 to 2.88 for the air smectites. Note that a small proportion of this magnesium is actually located in interlayer sites, in particular for the CO_2 smectite particles (<0.3, considering that cationic interlayer charge is < 0.6 per half unit-cell for a smectite). Fe^{3+} content varies from 0.71 to 0.96 for the CO_2 sample and from 0.27 to 0.45 for the air one. Neglecting the low amount of magnesium potentially located in interlayer sites, they exhibit an octahedral occupancy that appears intermediate between a trioctahedral smectite (three divalent cations per half-unit cell) and a

dioctahedral one (two trivalent cations), with an average value of 2.6 for the smectites formed under CO_2 and 2.8 for those formed under air. This implies a higher dioctahedral contribution for the CO_2 smectite, which is consistent with its higher Fe content. The presence of Al^{3+} is also observed for the two samples (0.16 for the CO_2 smectite and 0.12 for the air smectite). The major part of this aluminum is likely located in tetrahedral sites in replacement of Si^{4+} when a deficit of tetrahedral charge occurs. However, the presence of octahedral Al suggested by the Al^{3+} Al^{3+}-OH vibration near 2.2 µm observed by IR in the air sample remains unclear. It could be due to other Al-rich smectite layers or particles within the samples but not detected by TEM-EDX. The significant Al content in smectites and the presence of kaolinite particles compared with the low Al content in the initial olivine (254 ppm) indicate a strong concentration of this element in the alteration products during the weathering process under ambient air. Moreover, chromium and nickel are also detected but in very low abundances (0.01 for Cr^{3+} and <0.06 for Ni^{2+}). Finally, the smectite particles formed under CO_2 display a low tetrahedral charge deficit of - 0.08 (average value per half unit cell), compared -0.32 for the air smectite. The octahedral layer charge of these smectites cannot be calculated because of uncertainties of Mg location, in interlayer and/or octahedral sites. Nevertheless, as smectites have a layer charge deficit superior to 0.2 and a low tetrahedral charge, it is probable that a significant octahedral charge occurs in the CO_2 smectite. Moreover, considering the low contents of K^+ and Ca^{2+} interlayer cations in the CO_2 smectite, Mg^{2+} cations likely dominate the interlayer composition of this smectite. In contrast, Ca^{2+} likely dominates the interlayer composition of the air smectite.

6. Discussion

The precise characterization of the olivine samples after experiment indicates a strong influence of the atmospheric composition on the nature of the alteration products. The following section discusses the effect of a CO_2 atmosphere on the formation of clay minerals, amorphous silica and carbonates, and compares our results with the alteration products detected on Mars.

Clay mineral formation

The formation of a Mg/Fe^{3+}-rich smectite is clearly identified both under ambient air and under CO_2. Its presence is evidenced by IR data, with the appearance of a typical asymmetrical band at 2.31 µm with a shoulder at 2.29 µm attributed to Mg-OH vibrations in smectite (Cuadros et al., 2016). It is also confirmed by electron microscopy, with the development of numerous flaky particles observed as coating on the olivine grains or/and on the silica spheres for the CO_2 sample. No smectite was detected by XRD, suggesting that its abundance is too low to be detected or that this phase is amorphous and therefore could be considered as a precursor. However, the detailed observation of the smectite flakes by HRTEM show clear stacked 001 fringes confirming the crystalline character of these particles (Fig. 6c). The comparison of the abundance of smectite particles observed by microscopy and of the intensity of the smectite infrared signature at 2.31 µm clearly shows that this mineral is significantly less abundant under CO_2 than under air. We note that the diagnostic band at 2.3 µm is similar in position and shape for both samples, thus suggesting a similar nature of the smectite. However, TEM-EDX analyses of particles allowed us to characterize more precisely the crystal chemistry of the smectite formed under the two atmospheres. In both cases, they appear intermediate between a trioctahedral Mg^{2+}-rich end-member with a high tetrahedral charge (saponite) and a dioctahedral Fe^{3+}-rich end-member with a low tetrahedral charge (likely Fe-montmorillonite). But a clear enrichment in Fe for the smectites formed under CO_2

is found (in average per half unit-cell: $Fe_{0.8}Mg_{1.7}$ under CO_2 against $Fe_{0.4}Mg_{2.6}$ under air). This enrichment in Fe for the CO_2 smectite compared to the air one could be explained both by the presence of Fe^{2+} cations in solution due to the soluble character of this element under anoxic condition (CO_2), and by the consumption of Mg^{2+} cations through precipitation of Mg-rich carbonate (hydromagnesite) in this experiment. Thereby, less Mg^{2+} and more Fe^{2+} is available for smectite formation and higher smectite Fe:Mg ratios are expected under CO_2.

Interestingly, no evidence of reduced iron is noted for the smectites formed under CO_2 despite the fact that anoxic conditions were maintained throughout the experiment, as shown by the Eh value of -46 mV measured at the end of the experiment. As reported in Chetmob et al. (2015) from IR spectra of $Fe^{2+}/Fe^{3+}/Mg^{2+}$ smectites, the $Fe^{2+}Fe^{2+}Fe^{2+}$-OH vibration in smectite is located at 2.36 µm and its presence in Fe/Mg smectite would induce a shift of the band at 2.31 µm toward higher values. Possible explanations for the absence of detected Fe^{2+} include the oxidation of it through the reduction of H_2O (with emission of H_2, as observed in Dehouck et al., 2014a), or a rapid oxidation of a Fe^{2+}-bearing smectite in our CO_2 sample upon exposure to ambient air (the transfer time between the glovebox and the IR spectrometer was less than an hour). This aspect being unclear, it will be important in future experiments to avoid any contact with O_2 before IR analyses.

Previous experiments presented in Dehouck et al. (2012, 2016) carried out at room temperature (15-20 °C) for 4 years with a low fluid / rock ratio (evaporitic environment)

under CO_2 show the formation of smectites displaying similar morphologies and IR spectral signature (2.29-2.31 µm band) (Dehouck et al. ., 2016). In this previous study, the chemical analysis of the smectite particles was not possible because of their small sizes. The alteration conditions are not quite the same but this similarity suggests that the difference in temperature and W/R ratio have no impact on the nature of the smectite. Moreover, the range of smectite compositions observed in our samples has been previously reported for synthetic smectites (e.g. Grauby et al., 1994) and for natural ones in weathering profiles of basic or ultrabasic rocks (Nahon and Colin 1982a; Nahon et al. 1982b, c; Colin et al. 1990; Gaudin et al. 2004a, 2004b, 2005). Their intermediate compositions would result in intimate mixtures of dioctahedral and trioctahedral domains within the smectite layers (Grauby et al., 1994; Gaudin et al., 2005; Cuadros, 2010). However, the ferric dioctahedral character of smectites produced by natural weathering appear generally much more pronounced than in our experiments (generally Fe > 1 atom per half unit-cell; e. g. Köster et al., 1999 or Gaudin et al., 2004a). This discrepancy observed between natural and experimental systems would be due to a difference of an open system. Indeed, as suggested by Grauby et al. (1994): "In closed experimental systems, ferric iron and magnesium are continuously available and may react simultaneously with silica. Whereas in lateritic weathering processes, magnesium is early leached from profiles and iron is incorporated in smectites, oxides or oxyhydroxides".

On Mars, Fe/Mg smectites are the most common clay mineral reported by orbital spectroscopy (e.g., Carter et al., 2013) and have been locally observed in-situ at Gale crater (Vaniman et al., 2014). According to Carter et al. (2013), Fe/Mg phyllosilicates are by far the most common hydrous mineral detected on Mars, totaling 89% of all exposures of hydrous minerals. They are interpreted as ferric smectites and Mg-rich smectite mixtures. Several studies suggest that the Fe-bearing smectites were initially formed under anoxic conditions as Fe^{2+}-bearing smectites during the Noachian and were oxidized into Fe^{3+}-bearing smectites

later in the Martian history (e.g., Catalano, 2013; Dehouck et al., 2016). Moreover, Carter et al. (2015) identified 120 mineralogical sequences on the Mars surface with Al-phyllosilicates overlying Fe/Mg smectites, suggesting a global weathering process on the surface of Mars. Michalski et al. (2015) showed from IR orbital data that alteration on Mars is accompanied by a strong Fe-Mg segregation. Indeed, most (≥70%) of Martian smectite clays appear particularly enriched in Fe (FeO/MgO >10) compared to the Martian basaltic protolith. Our experiments show that such enrichment in Fe is to be expected when clay minerals are formed by low-temperature weathering under a dense CO_2 atmosphere.

Al-bearing clays. Although the Al content measured for the initial olivine is very low (254 ppm), this element is detected in all the clay particles analyzed by TEM-EDX. Such Al concentration in clay minerals is classically observed for weathering and due to the particular insoluble character of this element at intermediate pH **and at mildly acidic conditions**. Some Al-rich particles interpreted as kaolinite are observed in the air sample and a significant amount of Al is measured in the Mg/Fe-smectites of both the air and CO_2 samples (up to 0.37 per half unit-cell). This Al occurrence is consistent with the band at 2.2 µm detected in the air sample and attributed to Al-OH vibration in smectite. Note that for the CO_2 sample, the Al-OH component could be masked by the broad band at 2.2 µm attributed to silica. Unfortunately, the very low abundance of this element in our experiments prevent us to discuss the possibility of a significant effect of a CO_2 atmosphere on its speciation. Future alteration experiments of Al-rich materials (such as feldspar minerals) will facilitate the characterization of its behavior.

Amorphous silica-rich phase

No evidence of a silica-rich phase was found in the air sample, whereas SEM and TEM petrological observations of the surfaces of the CO_2-olivine grains showed the

development of numerous very small (10-100 nm) amorphous silica-rich spheres. We interpret their presence under CO_2 and their absence under air as a consequence of the difference in pH conditions, the lower pH of the former favoring Mg^{2+} and Fe^{2+} leaching. The significant occurrence of this phase in the CO_2 sample is confirmed by the appearance of a broad infrared band near 2.2 µm attributed to Si-OH vibration in amorphous silica. Dehouck et al. (2014a) observed similar particles by TEM but their IR spectra did not show the diagnostic band at 2.2 µm, which suggests a higher maturity and/or a higher abundance of this material in the present study. The higher abundance is likely favored by a longer reaction time and the continuous stirring of the reactors. Indeed, stirring likely favors the removal of the silica-rich layer from the surface of the grains and thus limits the passivating effect of this layer, which in turn would allow more leaching to occur and more spherules to be formed. Such an amorphous Si-rich phase is often described as a passivating layer, which tends to decrease the dissolution rate of olivine and, in some cases, prevents the formation of any other secondary phase (e. g. King et al., 2010; Garcia et al., 2010; Daval et al., 2011). Therefore, it is possible that the development of the Si-rich phase in the CO_2 sample has contributed to decrease the abundance of the smectite phase compared to the air-sample.

Interestingly, a similar spectral signature attributed to opaline silica is frequently reported from orbital IR data of Mars (e.g., Carter et al., 2013). More particularly, it is identified in Valles Marineris (Milliken et al., 2008) where it is locally associated with Fe sulfate and interpreted as weathering products of basaltic materials. Silica deposits (as much as 91 wt. % SiO_2) near sulfate-rich soil deposits are also reported in Gusev crater by Squyres et al. (2008) and are this time interpreted as formed under hydrothermal conditions. However, opaline silica is also detected in several late-stage delta and alluvial fans dated to the Hesperian to Amazonian periods (Carter et al., 2012). More recently, amorphous silica was found at Gale crater by the Curiosity rover in association with detrital tridymite (Morris et al.,

2016), and within diagenetic halos interpreted as a late stage of Si-rich fluid circulation (Frydenvang et al., 2017). It is also believed to contribute to the poorly-understood amorphous component that has been detected in all samples analyzed so far by the CheMin instrument (e.g., Dehouck et al., 2014b; Rampe et al., 2017). Therefore, most of these studies suggest that the occurrences of amorphous silica on Mars are disconnected from the major clay forming period and generally associated with low water/rock ratio and late stage conditions. Nevertheless, as reported in McKeown et al. (2011), its spectral detection using the ~2.2 µm feature in Martian reflectance spectra is difficult when it is mixed with Al-OH-bearing clays. Thereby, in the study performed by McKeown, the detailed comparison of CRISM Martian spectra from the Al-clay-rich rock units at Mawrth Vallis with laboratory spectra of silica-clay mixtures showed that both AlOH- and SiOH-bearing minerals are actually present in this unit. Thus, our results showing that weathering under a CO_2 atmosphere form abundant amorphous silica could partly explain the numerous detections of this phase on Mars in low-T (surface or diagenetic context) and that its presence may not always be decoupled from smectite formation.

Carbonation

The formation of a significant amount of carbonate (3.45 wt %) interpreted as hydromagnesite is shown by IR, TGA and SEM in the CO_2 sample, whereas no evidence of such a mineral is detected for the air sample. This occurrence is consistent with geochemical models (e.g. Zolotov et al., 2016) but differs (1) from global martian orbital data which show only rare and local occurrences of carbonates (Carter et al., 2013) and (2) from our previous CO_2/H_2O experiments of ferro-magnesian silicate alteration (Dehouck et al., 2012; 2014a; 2016). Notice that Wray et al. (2016) suggest that carbonate is more common than previously thought, and is often intermixed with smectites. Concerning the comparison with our previous experiments,

in Dehouck et al. (2012, 2016) where weathering of olivine and pyroxene minerals in an evaporitic context (very low L/R ratio) is simulated, no evidence of carbonate formation is detected after 4 years of reaction with H_2O, whereas carbonate appears when H_2O_2 is added. Moreover, in the Dehouck et al. (2014a) study, where the experimental conditions are very similar to the present study, only traces of carbonate were found after 3 months of reaction (total inorganic carbon measured of 0.09 mg/g). Several parameters vary between the present experiment and the previous ones performed under CO_2 without H_2O_2: time of experiment (4 years, 3 months or 15.3 months), stirring, drying procedure (under ambient air, vacuum or CO_2), L/R ratio (evaporitic condition or L/R ratio of 10). Therefore, it remains difficult to characterize clearly the factors controlling the presence or the absence of carbonate in our experiments. For example, it is possible that in Dehouck et al. (2014a) carbonates were partly dissolved during the vacuum drying procedure. However, one factor proposed by the authors in this last study to explain partly the absence of carbonate is the passivating effect of the amorphous silica-rich layer on the silicate grain surfaces. Indeed, several experiments related to CO_2 sequestration at both elevated temperatures and elevated P_{CO2} (>100°C and >100 bars) also pointed the inhibiting effect of such a silica-rich layer on the carbonation process and the difficulty to model it using geochemical kinetic codes (Béarat et al., 2006; King et al., 2010; Garcia et al., 2010; Daval et al., 2011). These studies show how this process is partly governed by such passivating layers and by local interfacial mineral-solution environments that are not necessary representative of the bulk solution. This is particularly the case when the particles are not stirred during the experiment or during natural weathering. For example, Béarat et al. (2006) demonstrate how stirring favors the exposure of fresh reactive surfaces by abrasion of the passivating layers and therefore favors carbonation. In the same way, the present experiment which was constantly stirred clearly shows the formation of carbonate, whereas only low amounts of carbonates were detected in our previous experiments which

were not or rarely stirred (Dehouck et al., 2012, 2014a). Therefore, as previously reported in the literature for high T and P_{CO2} conditions, it is probable that stirring also favors carbonate formation in the present experiment. Additional experiments testing the effect of drying conditions, L/R ratio and composition of the initial material would be necessary to better constrain the parameters favoring carbonate formation both in experimental and natural settings.

7. Conclusions

This paper focuses on the influence of CO_2 on the weathering of a Fo_{90} olivine comparing two experiments conducted under CO_2 and ambient air. Experiments with near similar conditions were previously reported in Dehouck et al. (2014a), but the low quantity of alteration products formed after 3 months of reaction prevented their detailed characterization. In the present study, a time of experiment five times longer than previously (15.3 months) and a new experimental set up with a continuous stirring of reactors allowed us to increase kinetics and alteration progress and thus to investigate more in detail the nature of the alteration minerals. Our results confirm that the formation of a Fe/Mg smectite by weathering of a Fo_{90} olivine is compatible with a CO_2 atmosphere. The higher development of the smectitic flacks in these experiments compared to our previous studies allowed for the first time (1) to observe the stacking layers within the particles by HRTEM confirming their crystallized character and (2) to analyze their chemical compositions to obtain their chemical formulae (Table 3). They appear intermediate between a trioctahedral Mg-rich saponite and a dioctahedral ferric smectite. An interesting result obtained from these chemical data is a clear enrichment in iron for the smectite formed under CO_2 compared to that formed under ambient air. Indeed, the iron content in the CO_2 smectite is two times higher than in the air smectite, with 0.8 Fe and

0.4 Fe per average half unit-cell respectively. This Fe enrichment is consistent with the detection of abundant ferric smectites on Mars (e. g. Carter et al., 2013).

Moreover, the CO_2 atmosphere induces the development of numerous silica-rich spherical particles coated on the olivine grains, whereas such a phase appears absent under ambient air. Similar particles were already observed in Dehouck et al. (2014a) but with a non-diagnostic near-infrared spectral signature and their morphologies, less distinct, were described as "cotton-like". The silica-rich particles formed in the present experiment shows this time a 2.2 µm diagnostic band suggesting a higher maturity of these particles compared to the previous ones. The abundance of this phase suggests that its occurrence could be actually more abundant than previously reported for Mars, as suggested by the ubiquitous detection of amorphous material in the sedimentary rocks of Gale crater. A detailed study of spectra from the Al-clay-rich units of Martian weathering profiles as performed by McKeown et al. (2011) at Mawrth Vallis where silica was detected would be necessary to confirm it.

Captions

Fig. 1. Experimental set-up allowing both heating and continuous stirring of reactors during the experiments. A first experiment was conducted under CO_2 in a glove-box and a second one was conducted under ambient air (only one reactor under each atmosphere). Reactors were sealed shut but occasionally open for pH measurements during the experiment.

Fig. 2. Infrared spectra of the CO_2 and air samples compared to the initial olivine and USGS ones (Non: nontronite, Sap: saponite, Mnt: montmorillonite, Bei: beidellite, hMgs: hydromagnesite, Mgs: magnesite, Cal: calcite, Sid: siderite).

Fig. 3. Thermogravimetric analyses (TGA) and differential thermogravimetric (DTG) curves of the initial olivine, CO_2 and air samples. Chemical compounds in the off-gas (H_2O, CO_2) were measured by mass spectrometry in real-time along with each mass loss.

Fig. 4. Comparison of the XRD pattern of the initial olivine with those of the altered olivines (under CO2 and ambient air).

Fig. 5. SEM images of the CO_2 sample: flaky particles of smectite (a, b,), silica-rich spheres (c, d) developed on the olivine grain surfaces. Sometimes, smectite and silica-rich sphere appear developed together on a same olivine grain (e). Particles of Mg-rich carbonate are also observed (f).

Fig. 6. (a, b) TEM images and micro-diffraction pattern of the amorphous silica-rich spheres and (c) high-resolution TEM (HRTEM) of smectites in CO_2 sample. flakes of smectites appear developed either as coatings around the silica spheres (a) or directly on the olivine surfaces (Fig. b). An 1, 6: TEM-EDX data reported in Table 3, and Fig. 8.

Fig. 7. (a, b) SEM and (c, d, e) TEM images of the flaky particles of smectite developed on the olivine surfaces (An. 8: TEM-EDX data reported in Table 3 and in Fig. 8). (f) TEM image of pseudo-hexagonal particles interpreted as kaolinite.

Fig. 8. TEM-EDX data of the CO_2 (a) and air (b) samples. Virtual smectite end-members of a saponite (3.8 Si, 3 Mg per half unit-cell), a saponite-Fe^{2+}(3.8 Si, 3 Fe^{2+}), a nontronite (3.8 Si, 2 Fe^{3+}) and a smectite-Al (3.8 Si, 2.2 Al) are reported for comparison Analyzes (An) 1, 6, 8, 25, 33; see Figs. 6, 7, 8.

Table 1. Summary of experimental conditions in our previous alteration studies of Fe/Mg-rich silicates.

Table 2. Bulk chemical composition of the San Carlos initial olivine analyzed by ICP-OES and (*) Chemical formulae calculated on the basis of 11 oxygen from ICPO-ES and average TEM-EDX data. (**) Trace-elements are measured by ICP-OES using a standard addition method and appear relatively coherent compared with the ones reported by De Hoog et al. (2010) for the San Carlos Olivine.

Table 3. Chemical formulae of the smectite and kaolinite from TEM-EDX data and calculated on the basis of 11 and 7 oxygens respectively. (An = analyze; see Figs. 6, 7, 8 for An 6-8-25-33.

Appendix 1: Equipment used for analyses

The chemical composition of the bulk powder olivine was measured at the LPG-Nantes laboratory by Inductively Coupled Plasma-Optical Emission Spectrometry (ICP-OES, iCAP 6300 Radial, Thermo Scientific). Before analysis, sample was prepared by alkaline fusion with $LiBO_2$ at 1050°C and by digestion with HNO_3 (10 %). The standard addition method was used to quantify minor elements (Na, Al, Ca, Cr, Mn, Co).

Powder X-ray diffraction (PXRD) data were obtained at the IMN laboratory (Nantes, Frances) using a Brüker "D8 Advance" powder diffractometer operated in Bragg–Brentano geometry with a Cu anode sealed X-ray tube and a focusing Ge(111) primary monochromator (selecting the Cu Kα1 radiation; λ = 1.540598 Å). PXRD patterns were acquired between 3.5 and 70°2θ with steps of 0.0157° and a counting time per step of 0.8 s.

Near-infrared spectra of our initial and weathered powders were acquired at the LPGN laboratory (Nantes, France) using a Nicolet 5700 Fourier transform infrared spectrometer (FTIR) equipped with a tungsten-halogen white-light source, a CaF2 beam splitter and a DTGS detector. For each sample, the FTIR chamber was first purged for four minutes with dry and CO2-free air. Spectra presented in this paper are the average of 200 measurements in the wavelength range of 1–5 µm (10000–2000 cm^{-1}) with a resolution of 4 cm^{-1}. Background spectra were acquired using a Labsphere-Infragold reference, with a rough surface optimized for powder analyses. Data acquisition and background correction were done using the OMNIC software.

Thermogravimetric analyses (TGA) were performed at the IMN laboratory (Nantes, France) using a Setaram sensys evo TG-DSC 111 thermobalance and a Quadrupole Mass

Spectrometer - QMS 403 C Aëolos allowing to characterize chemical compounds in the off-gas in real-time along with each mass loss. The measure were performed at a heating rate of 5°C/min from 25 to 800 °C, under an argon flow of 20 mL/min. Data were then converted into differential thermogravimetric (DTG) curves.

TEM-EDX microanalyses were conducted at the CINaM laboratory (Marseille, France) on individual particles using a JEOL JEM 2011 TEM fitted with a X-Flash Silicon Drift Detector 5030 (Bruker). A drop of about 0.05 µl of dispersed clay sample in suspension of pure water was deposited on a copper grid (d = 3.5 mm) covered by a thin carbon film. Data collection parameters were set as follows: magnification of 50 000 x, 4L spot size, angular tilt of 20° toward the detector, time constant of 60 kcp.s^{-1}, energy range of 40 keV, and corrected counting time of 30 seconds. The beam diameter was set to ~ 20 nm (200 Å) in order to reach the smallest particles. The constant beam density was ~ 63.5 pA.cm^{-2}. O, Na, Mg, Al, Si, K, Ca, and Fe were quantified by applying the Bruker AXS MET line mark data quantification procedure, which is close to the original Cliff and Lorimer method (Cliff and Lorimer, 1975). In this procedure, the acquired EDX spectra are corrected by background subtraction (Bremsstrahlung calculation), Gaussian deconvolution, and k factors corrections using values previously calculated on layer silicate standards with known homogeneous compositions (Berthonneau et *al*., 2014).

REFERENCES

Béarat, H., McKelvy, M. J., Chizmeshya, A. V., Gormley, D., et al., 2006. Carbon sequestration via aqueous olivine mineral carbonation: role of passivating layer formation. Environmental science & technology 40(15), 4802-4808.

Berthonneau, J., Grauby, O., Ferrage, E., Vallet, J. M., et al. 2014. Impact of swelling clays on the spalling decay of building limestones: insights from X-ray diffraction profile. European Journal of Mineralogy, 26, 643-656.

Bishop, J. L., Gates, W. P., Makarewicz, H. D., McKeown, et al., 2011. Reflectance spectroscopy of beidellites and their importance for Mars. Clays and Clay Minerals 59(4), 378-399.

Brindley, G.W., Brown, G., 1980. Crystal structures of clay minerals and their X-ray identification. Mineralogical Society, London, 495 p.

Carter J., Poulet F., Mangold N., Ansan V., et al., 2012. Composition of alluvial fans and deltas on Mars. In Lunar Planet. Sci. Conf. XLIII. #1978 (abstr.).

Carter, J., Poulet, F., Bibring, J. P., Mangold, N., et al., 2013. Hydrous minerals on Mars as seen by the CRISM and OMEGA imaging spectrometers: Updated global view. Journal of Geophysical Research: Planets, 1-29.

Carter, J., Loizeau, D., Mangold, N., Poulet, F., et al., 2015. Widespread surface weathering on early Mars: A case for a warmer and wetter climate. Icarus 248, 373-382.

Catalano, J.G., 2013. Thermodynamic and mass balance constraints on iron-bearing phyllosilicate formation and alteration pathways on early Mars. J. Geophys. Res.: Planets 118, 2124-2136.

Chemtob, S. M., Nickerson, R. D., Morris, R. V., Agresti, D. G., Catalano, J. G., 2015. Synthesis and structural characterization of ferrous trioctahedral smectites: implications for clay mineral genesis and detectability on Mars. Journal of Geophysical Research 120, 1119-1140, doi:10.1002/2014JE004763.

Chevrier, V., Rochette, P., Mathé, P. E., Grauby, O., 2004. Weathering of iron-rich phases in simulated Martian atmospheres. Geology 32(12), 1033-1036.

Cliff, G., and Lorimer, G. W., 1975. The quantitative analysis of thin specimens. Journal of Microscopy, 103: 203–207. doi:10.1111/j.1365-2818.1975.tb03895.x

Colin, F., Nahon, D., Trescase, J. J., Melfi, A., 1990. Lateritic weathering of pyroxenites at Niquelandia, Goias, Brazil: the supergene behavior of nickel. Econ. Geol. 85, 1010-1023.

Craddock, R. A., and Howard, A. D., 2002. The case for rainfall on a warm, wet early Mars. J. Geophys. Res., 107(E11), 5111, doi:10.1029/2001JE001505.

Craddock, R. A., Maxwell, T. A., Howard, A. D., 1997. Crater morphometry and modification in the Sinus Sabaeus and Margaritifer Sinus regions of Mars, J. Geophys. Res., 102, 13,321–13,340, doi:10.1029/97JE01084

Cuadros, J., 2010. Crystal-chemistry of mixed-layer clays. In: Interstratified Clay Minerals: Origin, Characterization and Geochemical Significance (Fiore, S., Cuadros, J., Huertas, F.J., editors), AIPEA Educational Series, (1), 11-33.

Daval, D., Sissmann, O., Menguy, N., Saldi, et al., 2011. Influence of amorphous silica layer formation on the dissolution rate of olivine at 90°C and elevated pCO_2. Chem. Geol. 284, 193-209.

Dehouck, E., Chevrier, V., Gaudin, A., Mangold, et al., 2012. Evaluating the role of sulfide-weathering in the formation of sulfates or carbonates on Mars: Geochimica et Cosmochimica Acta 90, 47-63.

Dehouck, E., Gaudin, A., Mangold, N., Lajaunie, L., et al., 2014a. Weathering of olivine under CO_2 atmosphere: A martian perspective. Geochimica et Cosmochimica Acta 135(0), 170-189.

Dehouck, E., McLennan, S. M., Meslin, P.-Y., Cousin, A., 2014b. Constraints on abundance, composition, and nature of X-ray amorphous components of soils and rocks at Gale crater, Mars, J. Geophys. Res. Planets, 119, doi:10.1002/2014JE004716.

Dehouck, E., Gaudin, A., Chevrier, V., Mangold, N., 2016. Mineralogical record of the redox conditions on early Mars. Icarus, 271, 67-75.

De Hoog, J. C., Gall, L., Cornell, D. H., 2010. Trace-element geochemistry of mantle olivine and application to mantle petrogenesis and geothermobarometry. Chemical Geology, 270(1), 196-215.

Ehlmann, B. L., Mustard, J. F., Murchie, S. L., Bibring, J.-P., et al., 2011. Subsurface water and clay mineral formation during the early history of Mars. Nature, 479, 53-60, doi:10.1038/nature10582.

Forget, F., Wordsworth, R., Millour, E., Madeleine, J.-B., et al., 2013. 3D modelling of the early martian climate under a denser CO_2 atmosphere: Temperatures and CO2 ice clouds. Icarus 222(1) Issue 1, 81-99.

Fritsch, E., Gaillou, E., Rondeau, B., Barreau, A., et al., 2006. The nanostructure of fire opal. Journal of Non-Crystalline Solids 352(38), 3957-3960.

Frydenvang, J., Gasda, P. J., Hurowitz, J. A., Grotzinger, J. P., et al., 2017. Diagenetic silica enrichment and late-stage groundwater activity in Gale crater, Mars. Geophysical Research Letters 44, 4716–4724, doi:10.1002/2017GL073323.

Garcia, B., Beaumont, V., Perfetti, E., Rouchon, et al., 2010. Experiments and geochemical modelling of CO_2 sequestration by olivine: potential, quantification. Applied Geochemistry 25(9), 1383-1396.

Gaudin, A., Grauby, O., Noack, Y., Decarreau, A., et al., 2004a. The actual crystal chemistry of ferric smectites from the lateritic nickel ore of Murin Murin (Western Australia). I-XRD and multi-scale chemical approaches. Clay Miner. 39, 301-315.

Gaudin, A., Petit, S., Rose, J., Martin, et al., 2004b. The actual crystal chemistry of ferric smectites from the lateritic nickel ore of Murrin Murrin (Western Australia). II-Spectroscopic (IR and EXAFS) approaches. Clay Miner. 39, 453-467.

Gaudin, A., Decarreau, A., Noack, Y., Grauby, O., 2005. Clay mineralogy of the nickel laterite ore developed from serpentinised peridotites at Murrin Murrin, Western Australia. Aust. J. of Earth Sciences 52(2), 231-241.

Gaudin, A., Dehouck, E., and Mangold, N., 2011. Evidence for weathering on early Mars from a comparison with terrestrial weathering profiles. Icarus 216(1), 257-268.

Gerdemann, S.J., O'Connor, W. K., Dahlin D. C., Penner L.R., et al., 2007. Ex situ aqueous mineral carbonation. Environ. Sci. Technol. 41, 2587-2593.

Giammar, D. E., Bruant, R. G., Peters, C. A., 2005. Forsterite dissolution and magnesite precipitation at conditions relevant for deep saline aquifer storage and sequestration of carbon dioxide. Chemical Geology 217(3), 257-276.

Grauby, O., Petit, S., Decarreau, A., Baronnet, A., 1994. The nontronite-saponite series: an experimental approach. Eur. J. Mineral. 6, 99-112.

Hynek, B. M., Beach, M., Hoke, M. R. T., 2010. Updated global map of Martian valley networks and implications for climate and hydrologic processes. J. Geophys. Res., 115, E09008, doi:10.1029/2009JE003548Jakovsky, B., and the MAVEN Science Team, 2017. MAVEN observations of Mars atmospheric loss and implications for long-term evolution. Lunar Planet. Sci. Conf. XLVIII., #1114 (abstr.).

King, H. E., Plümper, O., Putnis, A., 2010. Effect of secondary phase formation on the carbonation of olivine. Environmental science & technology 44(16), 6503-6509.

Kooli, F., Jones, W., 1997. Characterization and catalytic properties of a saponite clay modified by acid activation. Clay Minerals 32(4), 633-643.

Köster, H. M., Ehrlicher, U., Gilg, H. A., Jordan, R., et al., 1999. Mineralogical and chemical characteristics of five nontronites and Fe-rich smectites. Clay minerals 34, 579-599.

Mangold, N., S. Adeli, S., Conway, Ansan, V., Langlais, B., 2012. A chronology of early Mars climatic evolution from impact crater degradation. J. Geophys. Res. 117, E04003, doi:10.1029/2011JE004005.

Marcucci, E.C., Hynek, B.M. 2014. Laboratory simulations of acid-sulfate weathering under volcanic hydrothermal conditions: Implications for early Mars, J. Geophys. Res. Planets 119, doi:10.1002/2013JE004439.

McKeown, N., Bishop, J. L., Cuadros, J., Hillier, S., et al., 2011. Interpretation of reflectance spectra of clay mineral-silica mixtures: Implications for Martian clay mineralogy at Mawrth Vallis. Clays and Clay Minerals 59(4), 400-415.

Michalski, J. R., Cuadros, J., Bishop, J. L., Dyar, et al., 2015. Constraints on the crystal-chemistry of Fe/Mg-rich smectitic clays on Mars and links to global alteration trends. Earth and Planetary Science Letters 427, 215-225.

Milliken, R. E., Swayze, G. A., Arvidson, R. E., Bishop, J. L., Clark, R. N., et al., 2008. Opaline silica in young deposits on Mars. Geology 36(11), 847-850.
Montoya, C., Lanas, J., Arandigoyen, M., Navarro, I., et al., 2003. Study of ancient dolomitic mortars of the church of Santa María de Zamarce in Navarra (Spain): comparison with simulated standards. Thermochimica acta 398(1), 107-122.
Morris, R.V., Vaniman, D. T., Blake, D. F., Gellert, R., Chipera, S. J., Rampe, E. B., et al., 2016. Silicic volcanism on Mars evidenced by tridymite in high-SiO_2 sedimentary rock at Gale crater. PNAS 2016 113 (26), 7071-7076. Nahon, D., Colin, F., 1982a. Chemical weathering of orthopyroxenes under lateritic conditions. Am. J. Sci. 282, 1232-1243.
Nahon, D., Colin, F., Tardy, Y., 1982b. Formation and distribution of Mg, Fe, Mn-smectites in the first stages of the lateritic weathering of forsterite and tephroite. Clay Miner. 17, 339-348.
Nahon, D., Paquet, H., Delvigne, J., 1982c. Lateritic weathering of ultramafic rocks and the concentration of nickel in the Western Ivory Coast. Econ. Geol. 77, 1159-1175.
Pelletier, M., Michot, L. J., Barrès, O., Humbert, B., Petit, S., et al., 1999. Influence of KBr conditioning on the infrared hydroxyl-stretching region of saponites. Clay Minerals 34(3), 439-445.
Peretyazhko, T. S., Sutter, B., Morris, R. V., Agresti, D. G., et al., 2016. Smectite formation from basaltic glass under acidic conditions on Mars. Geochimica & Cosmochimica Acta 173, 37-49.
Poulet, F., Bibring, J. P., Mustard, J. F., Gendrin, A., et al., 2005. Phyllosilicates on Mars and implications for early martian climate. Nature 438, 623-627.
Rampe, E.B., Ming, D.W., Blake, D.F., et al., 2017. Mineralogy of an ancient lacustrine mudstone succession from the Murray formation, Gale crater, Mars. Earth and Planetary Science Letters 471, 172-185, doi:10.1016/j.epsl.2017.04.021.
Rondeau, B., Fritsch, E., Guiraud, M., Renac, C., 2004. Opals from Slovakia ("Hungarian" opals): a re-assessment of the conditions of formation. European Journal of Mineralogy 16, 789-799.
Schröder, C., Klingelhoefer, G., Tremel, W., 2004. Weathering of Fe-bearing minerals under Martian conditions, investigated by Mössbauer spectroscopy. Planetary and Space Science 52 (11), 997-1010.
Squyres, S. W., Arvidson, R. E., Ruff, S., Gellert, R., et al., 2008. Detection of silica-rich deposits on Mars. Science 320(5879), 1063-1067.
Tosca, N. J., McLennan, S. M., Lindsley, D. H., Schoonen, M. A., 2004. Acid-sulfate weathering of synthetic Martian basalt: The acid fog model revisited. Journal of Geophysical Research: Planets, 109(E5), doi:10.1029/2003JE002218.
Vaniman, D. T., Bish, D. L., Ming, D. W., Bristow, T.F. et al., 2014. MSL Science Team. Mineralogy of a mudstone at Yellowknife Bay, Gale crater, Mars. Science 343, doi:10.1126/science.1243480.
Zolotov, M.Y., Mironenko, M.V., 2016. Chemical models for martian weathering profiles: Insights into formation of layered phyllosilicate and sulfate deposits. Icarus 275, 203-220.

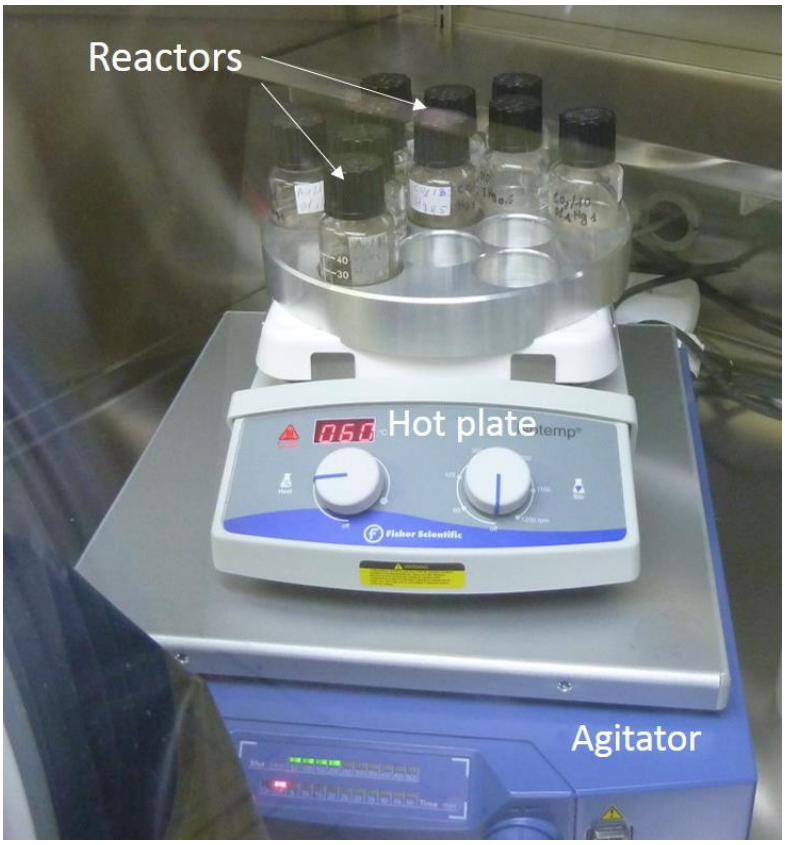

Fig. 1

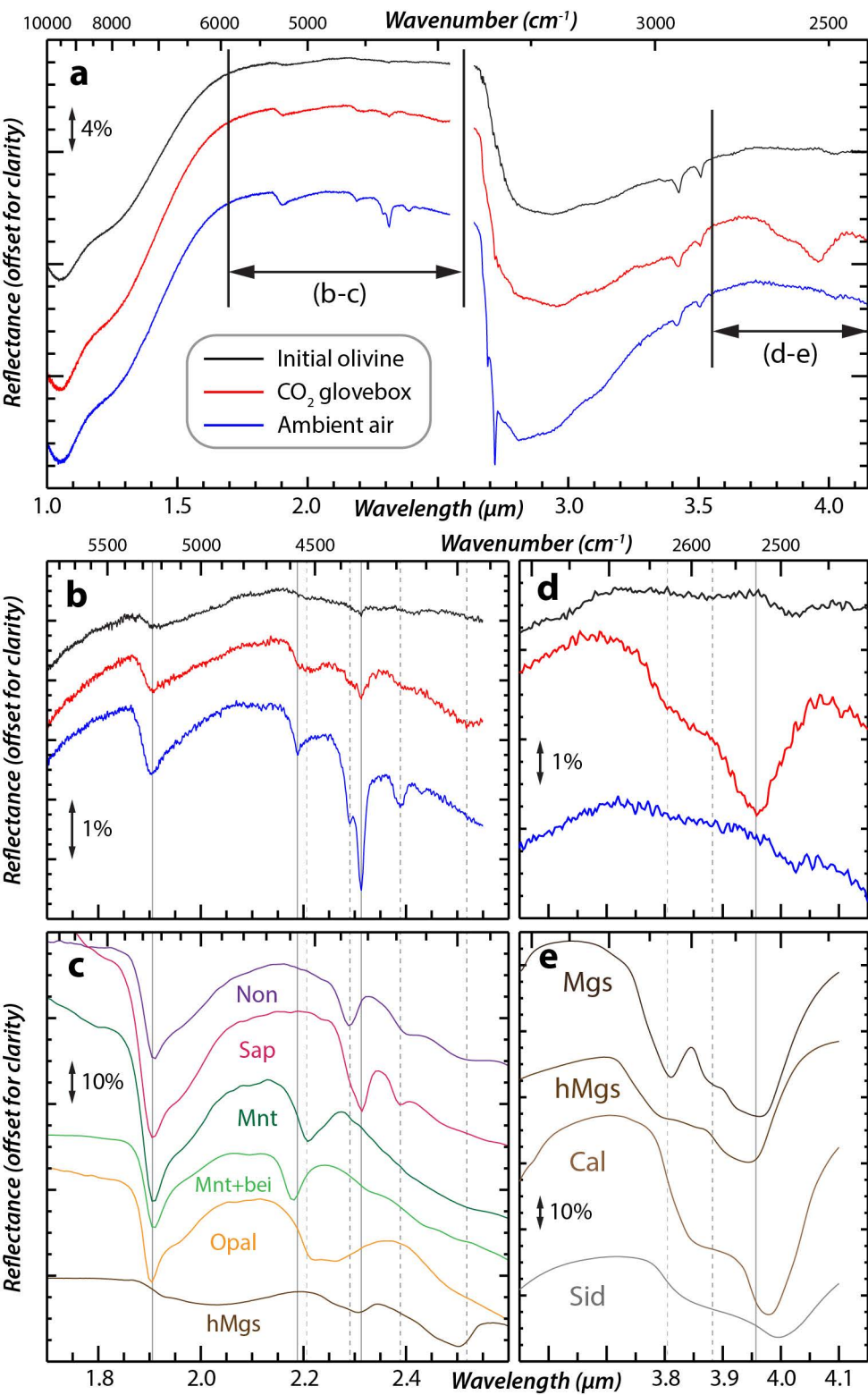
10000
8000
6000
5000
Wavenumber (cm-1)
3000
2500
a
4%
(b-c)
(d-e)
Initial olivine
CO2 glovebox
Ambient air
Reflectance (offset for clarity)
1.0
1.5
2.0
Wavelength (μm)
3.0
3.5
4.0
5500
5000
4500
Wavenumber (cm-1)
2600
2500
b
1%
d
1%
c
Non
Sap
Mnt
Mnt+bei
Opal
hMgs
10%
e
Mgs
hMgs
Cal
10%
Sid
1.8
2.0
2.2
2.4
Wavelength (μm)
3.8
3.9
4.0
4.1

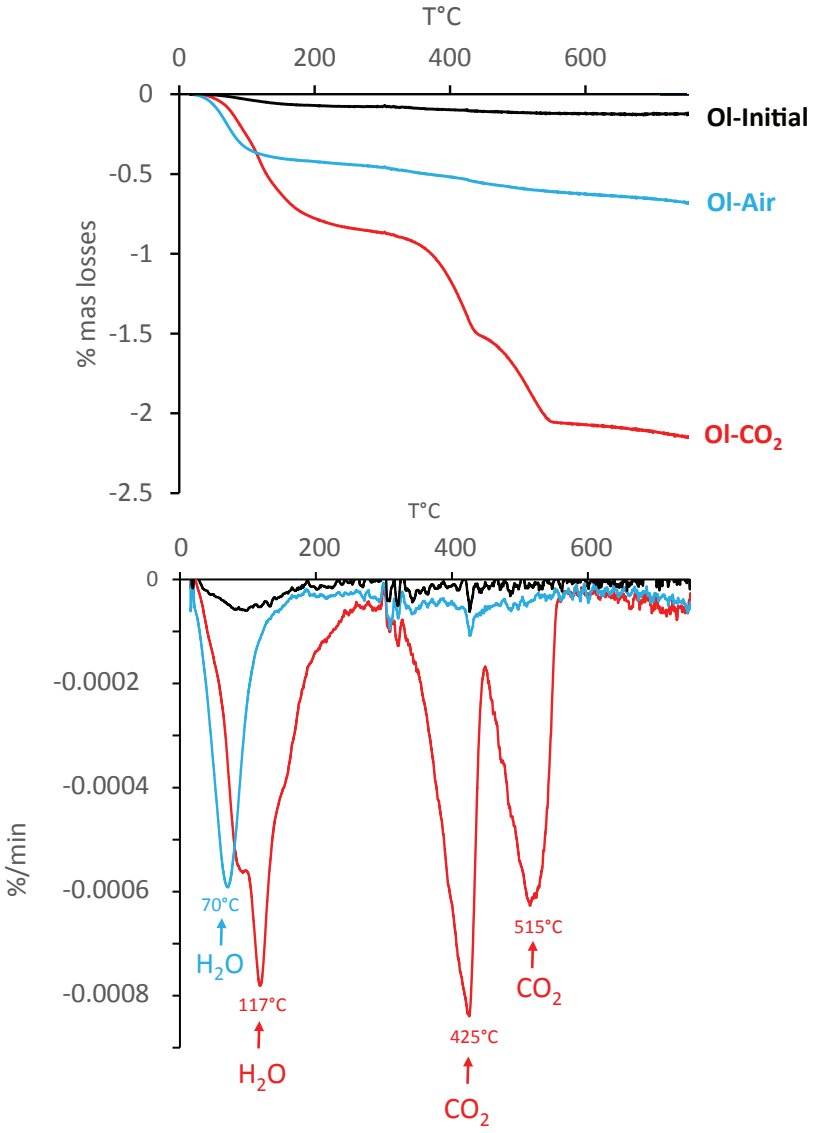
T°C
0
200
400
600
0
-0.5
-1
-1.5
-2
-2.5
% mas losses
Ol-Initial
Ol-Air
Ol-CO2
T°C
0
200
400
600
0
-0.0002
-0.0004
-0.0006
-0.0008
%/min
70°C
H2O
117°C
H2O
425°C
CO2
515°C
CO2

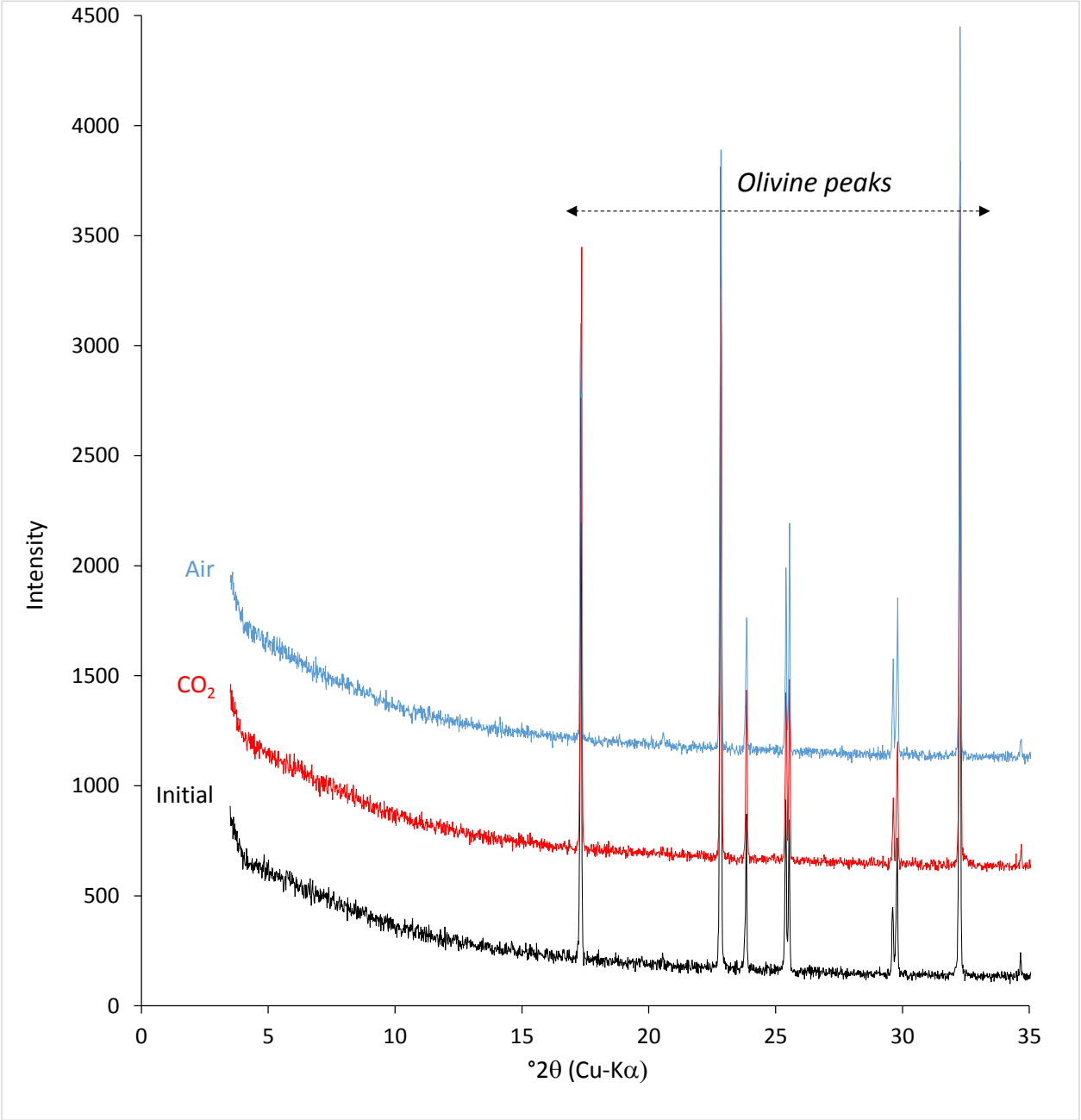
4500
4000
3500
3000
2500
2000
1500
1000
500
0
Intensity
Olivine peaks
Air
CO2
Initial
0
5
10
15
20
25
30
35
°2θ (Cu-Kα)

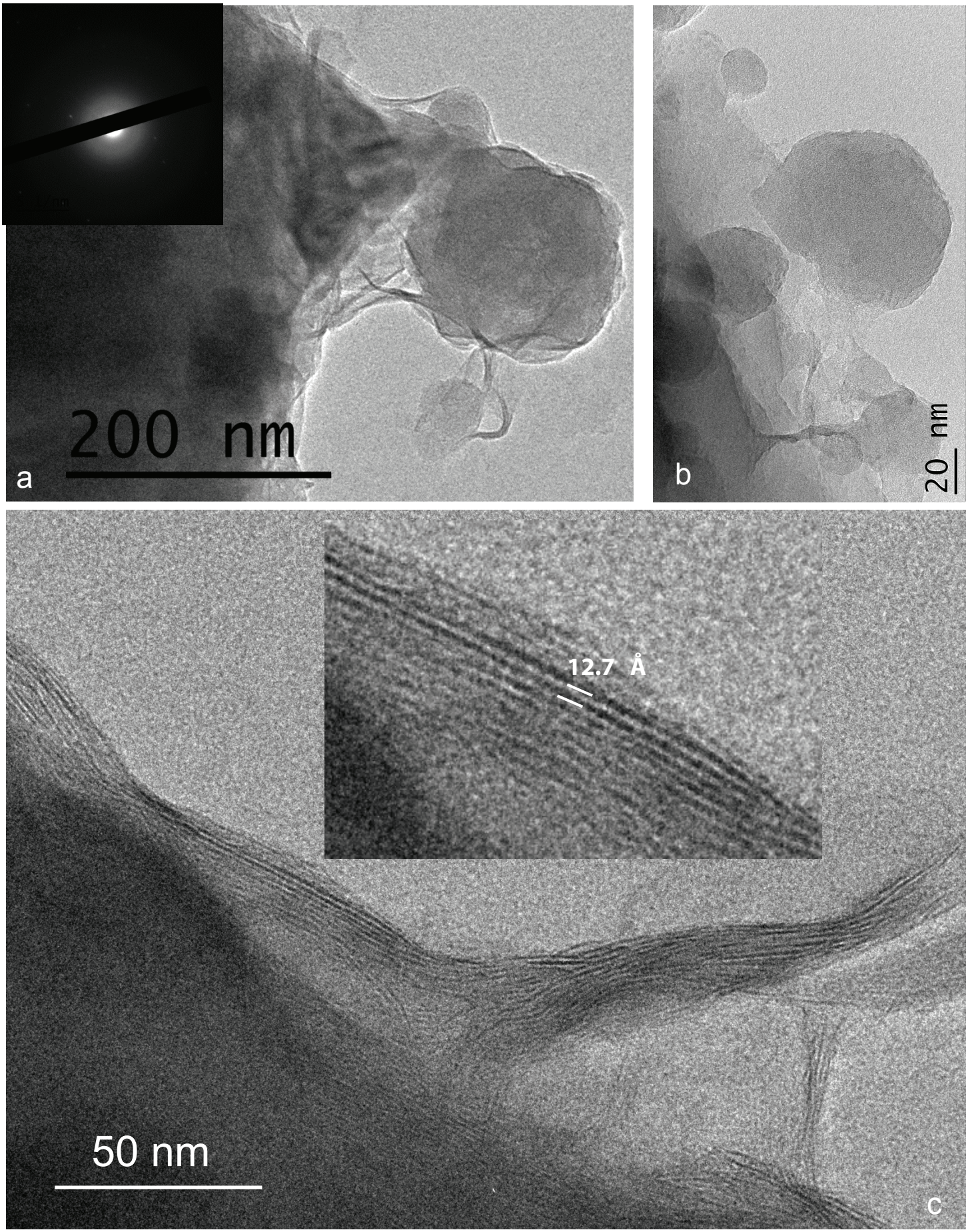
200 nm
a
b
20 nm
12.7 Å
50 nm
c

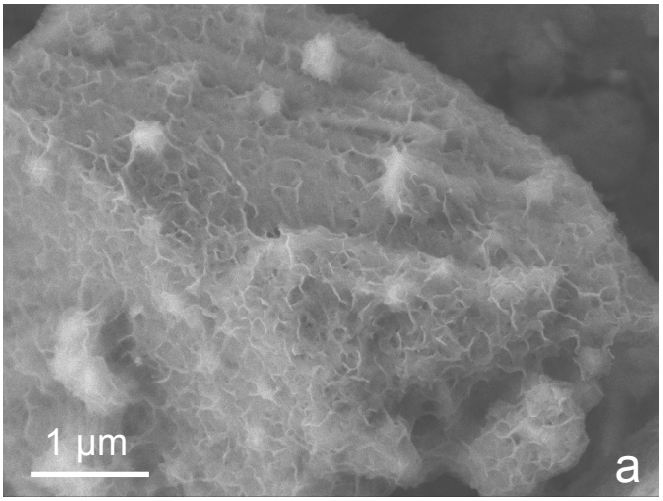
1 µm
a

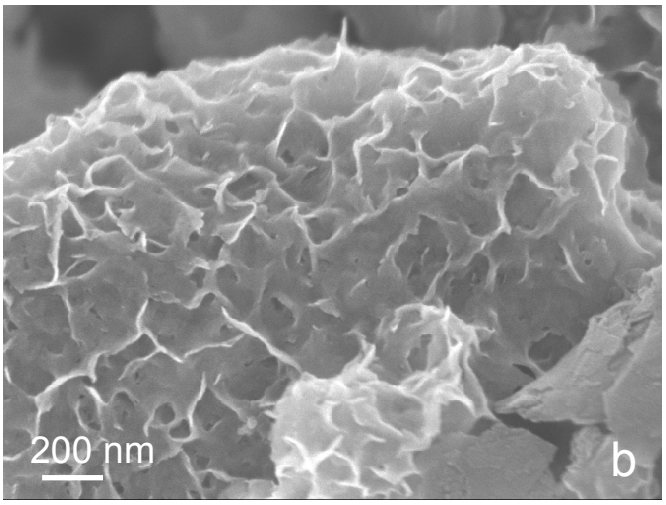
200 nm
b

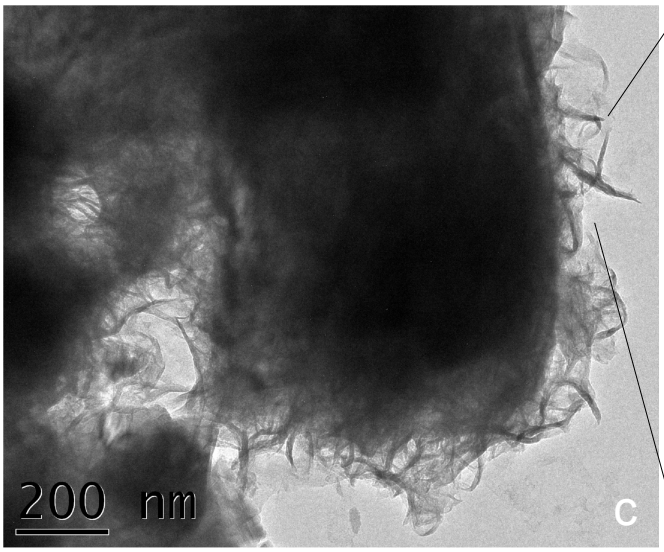
200 nm
c

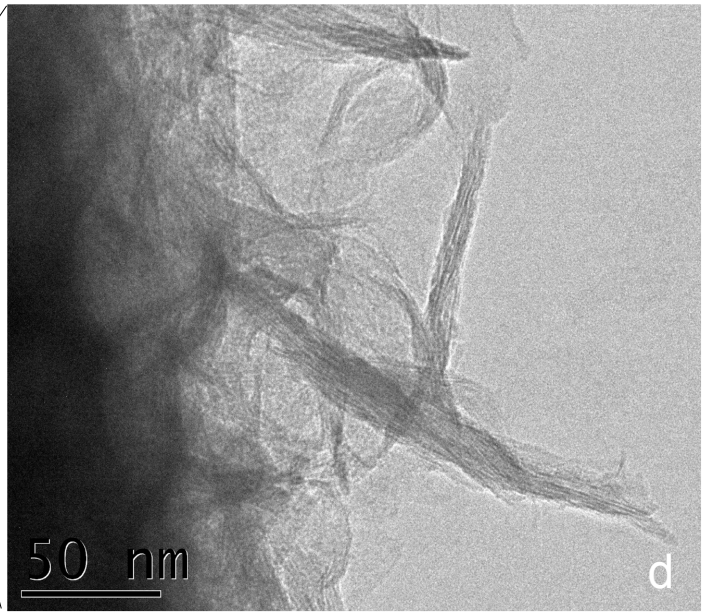
50 nm
d

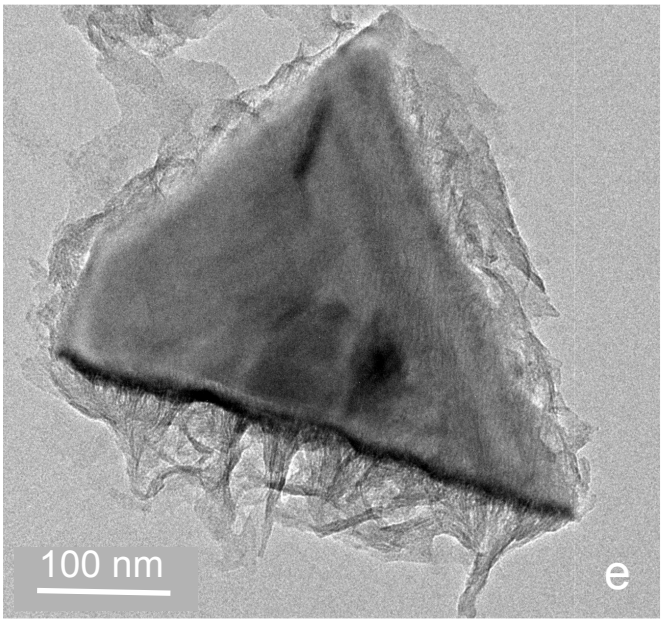
100 nm
e

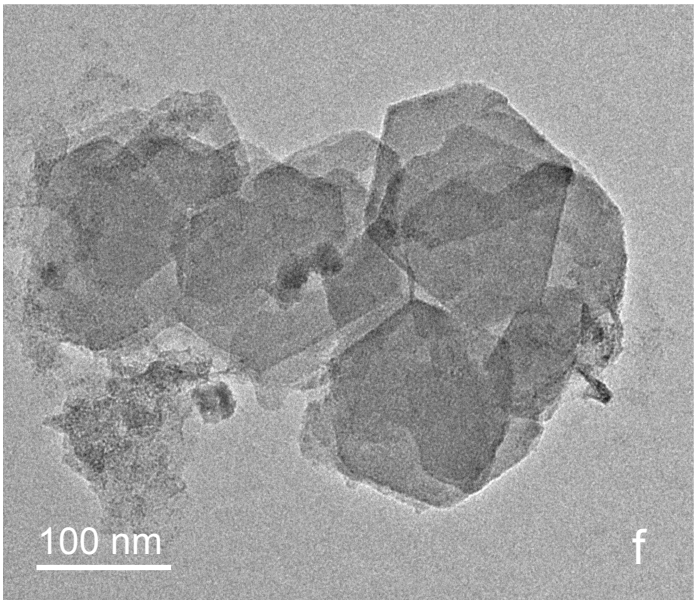
100 nm
f

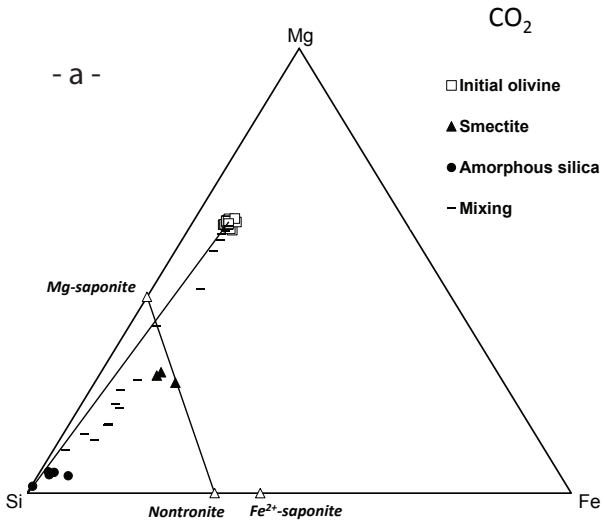
CO_2
- a -
Mg
Initial olivine
Smectite
Amorphous silica
Mixing
Mg-saponite
Si
Fe
Nontronite
Fe^{2+}-saponite

Ambient air

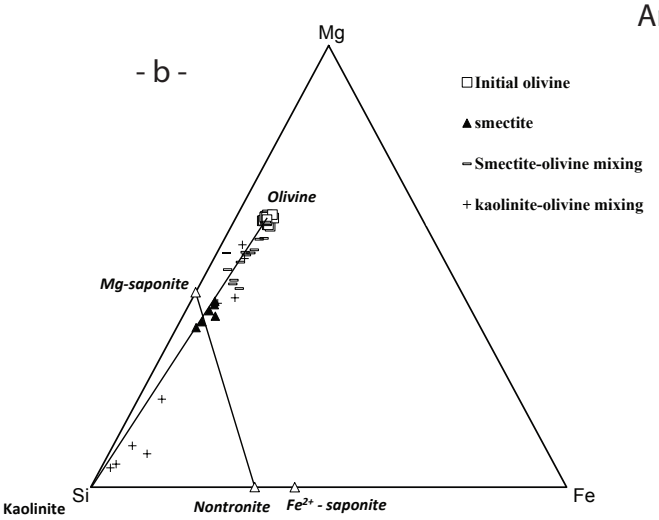
- b -
Mg
Initial olivine
smectite
Smectite-olivine mixing
kaolinite-olivine mixing
Olivine
Mg-saponite
Si
Fe
Kaolinite
Nontronite
Fe^{2+} - saponite

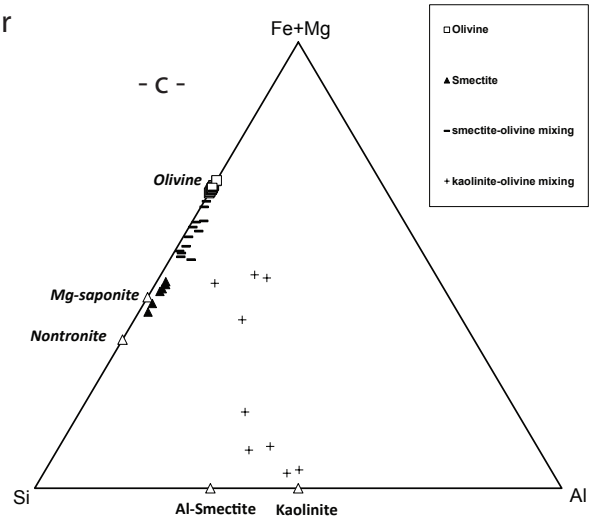
- c -
Fe+Mg
Olivine
Smectite
smectite-olivine mixing
kaolinite-olivine mixing
Olivine
Mg-saponite
Nontronite
Si
Al
Al-Smectite
Kaolinite

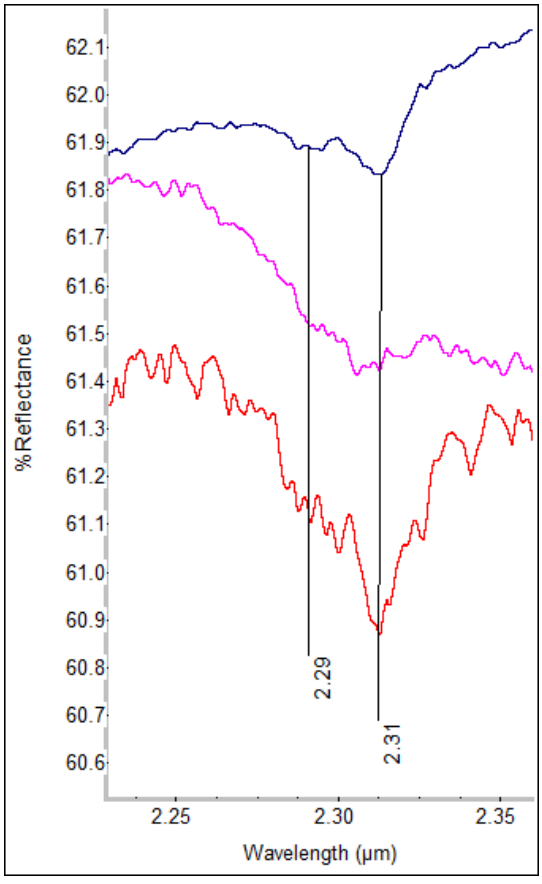

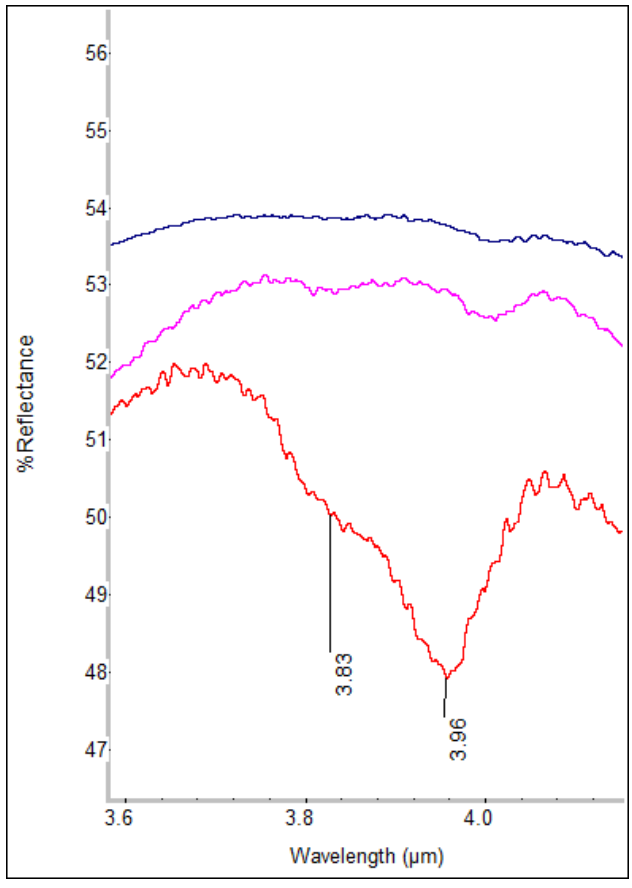

Dehouck et al. (2012): 4 years, very low W/R (evaporite), no stirred

Dehouck et al. (2014): 3 months, W/R=10, briefly daily manually stirred

This study: 14 months, W/R=10, continuous stirring